How solar cell efficiency is governed by the $\alpha\mu\tau$ product

Pascal Kaienburg,[1,2,*] Lisa Krückemeier,[1] Dana Lübke,[1] Jenny Nelson,[3] Uwe Rau,[1] and Thomas Kirchartz[1,4,†]

[1]*IEK5-Photovoltaics, Forschungszentrum Jülich, 52425 Jülich, Germany*

[2]*Clarendon Laboratory, Department of Physics, University of Oxford, Parks Road, OX1 3PU Oxford, United Kingdom*

[3]*Department of Physics and Centre for Plastic Electronics, Imperial College London, London SW7 2AZ, United Kingdom*

[4]*Faculty of Engineering and CENIDE, University of Duisburg-Essen, Carl-Benz-Strasse 199, 47057 Duisburg, Germany*

(Received 18 September 2019; accepted 15 March 2020; published 30 April 2020)

The interplay of light absorption, charge-carrier transport, and charge-carrier recombination determines the performance of a photovoltaic absorber material. Here we analyze the influence on the solar-cell efficiency of the absorber material properties absorption coefficient α, charge-carrier mobility μ, and charge-carrier lifetime τ, for different scenarios. We combine analytical calculations with numerical drift-diffusion simulations to understand the relative importance of these three quantities. Whenever charge collection is a limiting factor, the $\alpha\mu\tau$ product is a good figure of merit (FOM) to predict solar-cell efficiency, while for sufficiently high mobilities, the relevant FOM is reduced to the $\alpha\tau$ product. We find no fundamental difference between simulations based on monomolecular or bimolecular recombination, but strong surface-recombination affects the maximum efficiency in the high-mobility limit. In the limiting case of high μ and high surface-recombination velocity S, the α/S ratio is the relevant FOM. Subsequently, we apply our findings to organic solar cells which tend to suffer from inefficient charge-carrier collection and whose absorptivity is influenced by interference effects. We estimate that a modest increase in absorption strength by a factor of 1.5 leads to a relative efficiency increase of more than 10% for state-of-the-art organic solar cells.

DOI: 10.1103/PhysRevResearch.2.023109

I. INTRODUCTION

Three different physical mechanisms constitute the conversion of solar radiation into electrical energy by a solar cell: (i) the absorption of solar photons by the absorber material of the solar cell; (ii) the transport of photogenerated free charge carriers, electrons, and holes, towards the contacts; and (iii) the recombination of electrons and holes as the major loss mechanism. These three mechanisms are directly related to three quantities that are independently measurable for any absorber material: (i) the absorption coefficient $\alpha(E)$, a spectral quantity dependent on the photon energy E, (ii) the charge-carrier mobilities of electrons μ_n and holes μ_p, and (iii) the recombination rate of the charge carriers, often expressed by the (potentially charge-carrier density-dependent) carrier lifetime τ. All three quantities directly relate to the efficiency of the solar cell insofar that the higher these quantities are, the higher is the efficiency of the device. [1] In turn, suboptimal values of these three material quantities can constitute a major source of discrepancy between the actually attained solar-cell efficiency and the theoretical Shockley-Queisser limit [2–5].

Since the three quantities represent three different mechanisms within the solar cell, their combined influence on the efficiency is complex. For aspects related to the collection efficiency of charge carriers, the product of mobility and lifetime entering into the diffusion length [6–9] or the drift length [10] yields a good figure of merit (FOM), implying that a low mobility can be compensated by a high lifetime and vice versa. However, diffusion or drift lengths are always rated with respect to the absorber thickness which in turn has to be adapted to the absorption coefficient α. Thus, the product $\alpha\mu\tau$ would represent a more general figure of merit for the solar-cell efficiency. It is also understood that an increase in any of the three quantities is generally beneficial for solar-cell performance. However, it is not clear *a priori* whether for a given solar-cell material, e.g., an order of magnitude increase in lifetime would be similarly useful for efficiency as an order of magnitude increase in the absorption coefficient. Thus, while the qualitative importance of the three parameters is undisputed, the quantitative change in efficiency when improving either of these three parameters only follows from numerically solving a set of coupled differential equations [11–15] known as the drift-diffusion model. One might therefore argue that improving any of the three parameters is generally good for the solar-cell efficiency, but by how much the efficiency will change precisely depends on so many aspects that generic answers will be impossible.

Being quantitative and generic when approaching this problem is therefore challenging. The current paper aims to approach this challenge using a combination of (i) briefly reviewing what we already know, (ii) studying patterns in sets of many numerical simulations with variations in all three

*pascal.kaienburg@physics.ox.ac.uk
†t.kirchartz@fz-juelich.de

parameters, and (iii) by using the obtained understanding in a practical example involving organic solar cells. The main result of the study is that for solar cells with collection issues, the efficiency at the optimum thickness is relatively constant for $\alpha\mu\tau = \text{const}$. If, however, charge collection is efficient, the mobility is no longer relevant and the efficiency will remain constant for a constant $\alpha\tau$ product. These statements hold true as long as bulk recombination described by a constant lifetime dominates recombination. For situations where bimolecular recombination dominates, analogous statements can be made and for cases where surface recombination dominates, efficiency will become independent of bulk lifetime. In that case the interface characteristics between absorber and contacts become relevant in addition to the bulk properties of the absorber. Specifically, the α/S ratio, with the surface-recombination velocity S, governs the solar-cell efficiency for high μ and high S. Thus, we note that despite the complexity of the problem, the relation of efficiency and the three material parameters α, μ, and τ becomes relatively simple once the comparison is not done at constant thickness but rather at the thickness where efficiency peaks. In the following, we start by briefly reviewing two known relations that motivate our work: These are (i) the relation between efficiency and the mobility-lifetime $\mu\tau$ product, which controls charge collection, and (ii) the relation between efficiency and the product of absorption coefficient and lifetime ($\alpha\tau$) which controls absorption and recombination and therefore efficiency in the limit of high mobilities.

II. BACKGROUND: $\mu\tau$ PRODUCT

The mobility-lifetime product $\mu\tau$ is a well-known photovoltaic concept [13] and enters into both the equations for the drift length [10,16] as well as for the diffusion length [6–9]. The $\mu\tau$ product therefore affects charge collection independently from the exact band diagram of the solar cell [17]. Figure 1 shows the results of numerical drift-diffusion simulations [11,13,14], which illustrate the correlation between the $\mu\tau$ product and the key performance parameters of a *p-i-n* solar cell with a fully depleted absorber layer. Either the mobility (blue, open circle) or the lifetime (red, solid circle) is varied along one curve in Figs. 1(a)–1(d), while the other parameter—as well as the absorption coefficient—is fixed. Note that in both experiments and simulations, the values of mobility and lifetime can generally be controlled independently. We assumed the mobility and lifetime to be independent of charge-carrier density implying linear transport and recombination dynamics. The simulation parameters are given in the figure. Figure 1(a) exhibits a very similar behavior of the short-circuit current density J_{sc} if either μ or τ is varied. As one may expect, the $\mu\tau$ product governing charge collection is the relevant figure of merit determining J_{sc} for an unchanged absorptance that is determined by the fixed absorber thickness and absorption coefficient. For very low and very high values of the $\mu\tau$ product, the J_{sc} saturates but depends linearly on the logarithm of the $\mu\tau$ product in the intermediate regime. The trend for the fill factor in Fig. 1(b) is generally like that of the J_{sc}. Note that a more comprehensive analysis in an earlier work of ours [18] showed that mobility and lifetime are not equally important for the resulting

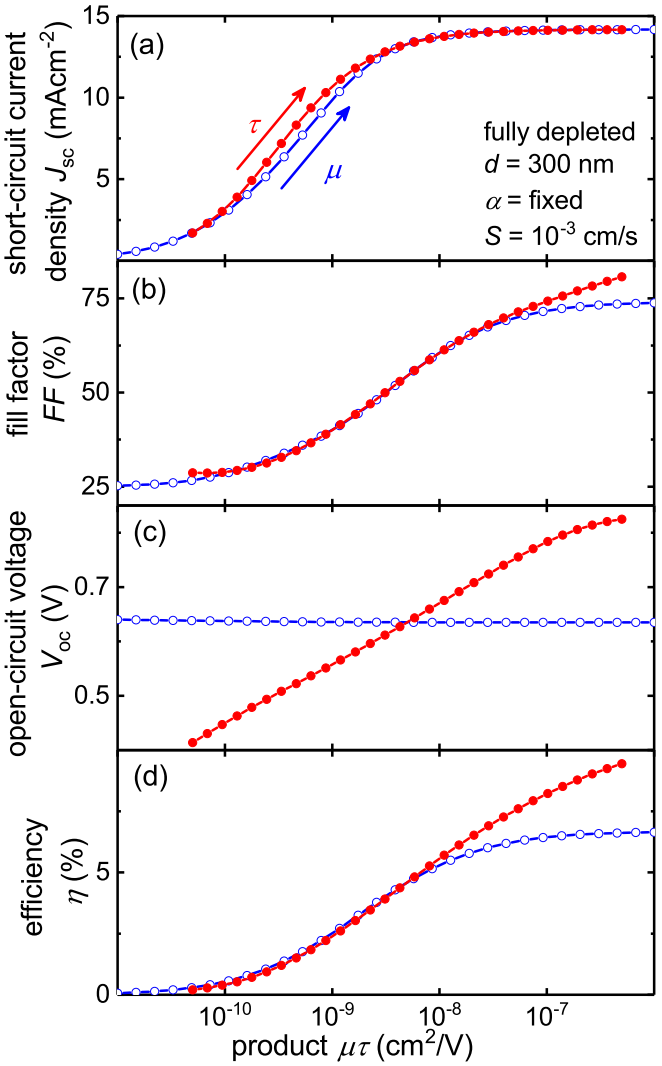

FIG. 1. Influence of the $\mu\tau$ product on the performance of a *p-i-n* solar cell illustrated with numerical drift-diffusion simulations [11,13,14]. The absorber layer is fully depleted. Recombination is governed by Shockley-Read-Hall recombination, characterized by the lifetime τ via the recombination rate $R = n\tau^{-1}$. The simple scenario assumes a vanishingly small surface recombination $S = 10^{-3}$ cm/s, a fixed absorption coefficient, and a fixed—and thus unoptimized—thickness of $d = 300$ nm. The band gap is set to $E_g = 0.9$ eV with Schottky barriers of $\varphi = 0.1$ eV. The dielectric constant of $\epsilon_r = 3.5$ reflects organic materials. Either the lifetime is fixed at $\tau = 10^{-5}$ s and the mobility is varied (blue, open circle) from $\mu = 10^{-6}$ to 10^{-1} cm^2/(V s) or $\mu = 5 \times 10^{-4}$ cm^2/(V s) is fixed and τ is varied (red, solid circle) between 10^{-7} and 10^{-3} s. The (a) J_{sc} and (b) fill factor behave similarly for a variation of μ or τ. The (c) V_{oc} remains constant for a variation of μ but varies with τ, which also explains the different saturation levels of the fill factor [19,20]. (d) The efficiency scales well with the $\mu\tau$ product for low and intermediate $\mu\tau$ values making it a reasonable figure of merit in this regime. At high $\mu\tau$ values where charge collection is optimal, longer lifetimes further increase the efficiency via the V_{oc}, but the product of μ and τ loses its significance.

fill factor, as might be suggested by the example shown in Fig. 1(b). In the saturation regime at high $\mu\tau$ values, the two cases behave differently because the maximum attainable fill

factor depends on the open-circuit voltage (V_{oc}) [19,20]. The V_{oc} in turn depends on the bulk lifetime τ [21–23] but is—as long as surface recombination is negligible—independent of the mobility μ [24]. Consequently, also the two curves for the efficiency (η) in Fig. 1(d) diverge and longer lifetimes lead to higher efficiencies, which is not the case for higher mobilities. In other words, for low- and intermediate-$\mu\tau$ products, charge-carrier collection limits the device performance and the $\mu\tau$ product governs the efficiency. For high-$\mu\tau$ products, a further increase in the value of $\mu\tau$ does not further improve charge-carrier collection and charge transport losses become negligible. However, charge-carrier recombination remains critical, so that only τ affects the efficiency instead of the product of μ and τ.

III. BACKGROUND: $\alpha\tau$ PRODUCT

After exemplifying how mobility and lifetime act on the solar-cell efficiency, we explore the importance of the absorption coefficient as the third critical material parameter for device performance. We start by examining the absorption coefficient of various organic and inorganic semiconductors in Fig. 2. The absorption coefficient can always be expressed as $\alpha = \alpha_0 f(E)$, where a function $f(E)$ defines the spectral shape and α_0 is a prefactor that determines the absolute value of α that reflects the absorption strength. Figure S1 in the Supplemental Material displays the absorption characteristics of further organic absorber materials [25]. The values of α at energies in the visible vary by more than an order of magnitude and reach the highest values for organic semiconductors. It has been shown that the absorption strength of certain semiconducting polymers can be tuned by simply changing the molecular weight [26] (MW), as is the case for thieno[3,2-b]thiophene-diketopyrrolopyrrole (DPPTTT) displayed in Fig. 2 resulting in an increase in α_0 by a factor of roughly 1.5.

In the following, we introduce the third bulk absorber parameter α_0 into our discussion of thin-film solar-cell efficiency. We consider an analytical treatment of the infinite-mobility case, which corresponds to the regime of high-$\mu\tau$ products in Fig. 1. In this scenario the efficiency does not vary with the mobility, but is governed by the interplay between recombination and absorption. We thus assess whether the absorption strength α_0 or the lifetime τ is more critical to the device performance. Based on the model of Blank *et al.* [29], the photocurrent as well as the radiative and nonradiative contributions to the recombination current are calculated as described in Ref. [1] and reproduced in Appendix A.

Figure 3(a) shows the thickness-dependent efficiency with (solid lines) and without (dashed lines) nonradiative recombination. Different lines show different absorption strengths α_0. For the nonradiative case, τ is varied along with α_0 such that the $\alpha_0\tau$ product remains constant in order to demonstrate its control over the efficiency. In the radiative limit, the lifetime τ is effectively set to infinity and only radiative recombination is considered. In that case the efficiency increases monotonously with thickness and finally saturates at the value of the Shockley-Queisser limit. The increase stems from a higher absorptance at larger thicknesses, which also

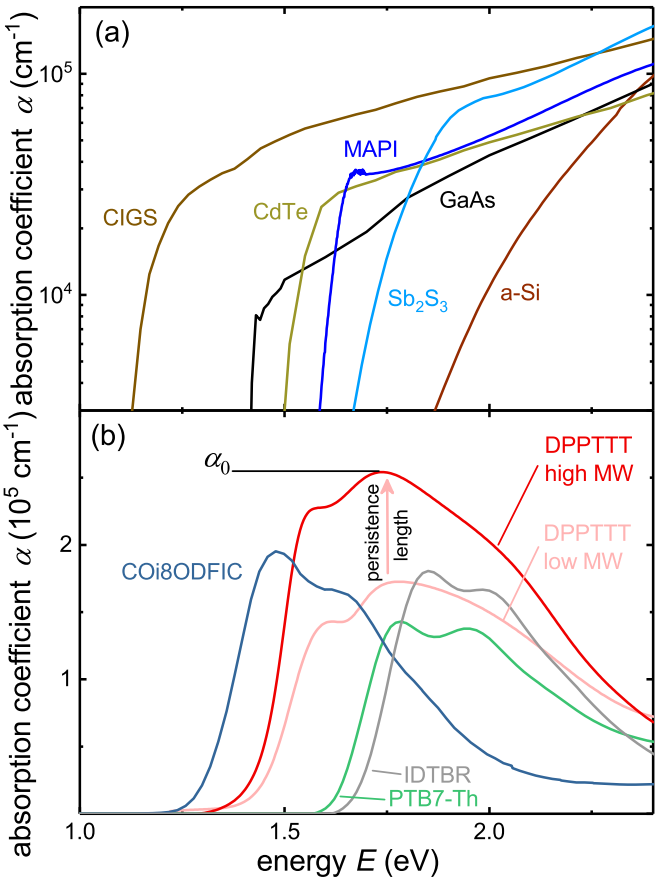

FIG. 2. Absorption coefficients of several (a) inorganic direct band gap (logarithmic scale) and (b) organic absorber materials (linear scale). The absorption spectra of organic materials are characterized by the maximum value α_0 that reflects the absorption strength. A change in the molecular weight (MW) of the semiconducting polymer DPPTTT was shown [26] to tune the absorption strength up to a factor of 1.5 via an increased persistence length [26]. The data for DPPTTT are obtained from Vezie and were published in Ref. [26] and data for IDTBR and PTB7-Th are taken from Ref. [27]. The data for GaAs, CIGS and CdTe are taken from [13], for MAPI are taken from Ref. [23], and for Sb_2S_3 are taken from Ref. [28].

explains the shift of the curves along the x axis for higher α_0. If nonradiative recombination is considered, the same holds true for the absorptance and thus J_{sc}. At the same time the volume in which charge carriers recombine increases with increasing thickness d, which causes a decrease in V_{oc} [30] (cf. Appendix A). This trade-off manifests in the emergence of an optimum thickness at which the efficiency peaks. Interestingly, even if the optimum thickness shifts for different values of α_0, the maximum efficiency remains constant as long as the $\alpha_0\tau$ product remains constant. In addition to α_0, the lifetime τ is varied over a wide range in Fig. 3(b), which yields a linear correlation between the $\alpha_0\tau$ product and the efficiency until the efficiency saturates at the Shockley-Queisser limit. In summary, if charge-carrier collection is ideal at all thicknesses, the optimum absorber thickness depends on the values of α_0 and τ. However, the maximum efficiency at the optimum absorber thickness only depends on the $\alpha_0\tau$ product of both quantities.

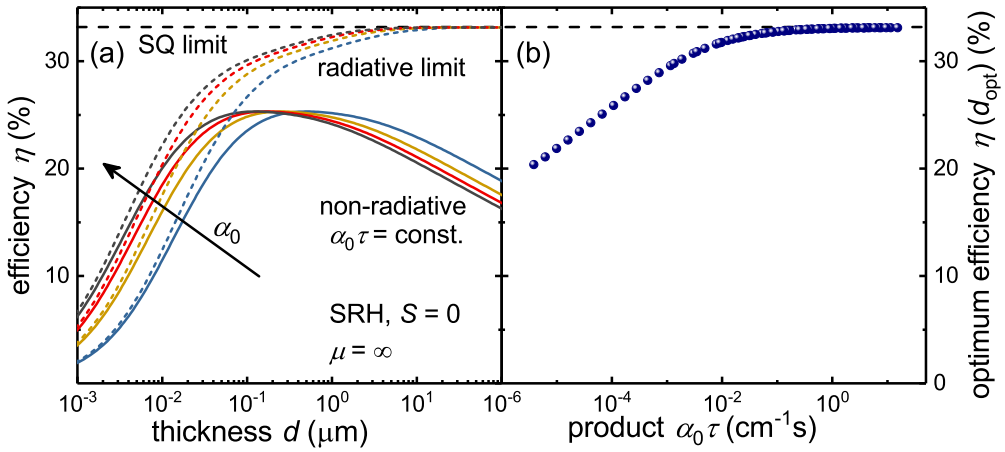

FIG. 3. Analytical calculations of the high-mobility limit following Refs. [1,29] for a fully depleted absorber layer with no recombination at the surfaces and Shockley-Read-Hall (SRH) recombination in the bulk. (a) The DPPTTT:PCBM standard spectrum (see Fig. 9 in Appendix A) is scaled by a factor $c_\alpha \in [0.5, 2]$. The lifetime τ is varied so that the $\alpha_0\tau$ product remains constant with $\tau(c_\alpha = 1) = 10^{-9}$ s. Lambertian light trapping [31] with unchanged reflectivity is taken as an optical model which does not consider interference. When nonradiative recombination is considered, an optimum thickness turns up as a result from the trade-off between an increasing volume for absorption and an increasing volume for recombination. The maximum efficiency is constant for different values of α_0, as long as the $\alpha_0\tau$ product is constant. (b) The efficiency at the optimum thickness scales with the $\alpha_0\tau$ product until the Shockley-Queisser limit is reached.

IV. RESULTS: $\alpha\mu\tau$ PRODUCT

After examining the $\mu\tau$ product for constant absorption and the $\alpha_0\tau$ product for infinite mobilities we now combine all three parameters and analyze the dependence of the efficiency on the product $\alpha_0\mu\tau$. Therefore we perform drift-diffusion simulations [11,13,14] with an optical model that includes interference, vary all three parameters over a wide range, determine the efficiency as a function of thickness, and then plot the efficiency at the optimum thickness as a function of $\alpha_0\mu\tau$. Details on the simulation parameters and underlying assumptions of the electrical drift-diffusion [11,13,14] and optical transfer-matrix method (TMM) [32] simulations can be found in Appendix A. The result for low surface-recombination velocities is shown in Fig. 4(a), where each data point results from a simulation of different combinations of a_0, μ, and τ at the optimized thickness. The dataset is divided via the color into simulations based on low [$\mu < 10^{-3}$ cm^2/(V s), red, open] and high [$\mu > 10^{-3}$ cm^2/(V s), blue, solid circle] mobilities. The efficiency of low-mobility devices in Fig. 4(a) nicely correlates with the here-defined figure of merit $\alpha_0\mu\tau$. In other words, the low degree of scatter of the red data points in panel (a) indicates that the efficiency of thin-film solar cells with low mobilities depends on $\alpha_0\mu\tau$ and thus jointly on all three absorber material parameters. In contrast to this, the high-mobility devices in blue show considerable scatter, meaning that for high mobilities, $\alpha_0\mu\tau$ is not a good figure of merit (FOM). Figure 4(b) contains the same dataset as Fig. 4(a), but the simulated efficiency is plotted against a different FOM ($\alpha_0\tau$), that excludes the mobility. As expected, the red data points are largely scattered in Fig. 4(b), because the mobility strongly affects the efficiency for low-mobility devices. However, the blue data points correlate well with $\alpha_0\tau$, making the $\alpha_0\tau$ product a good FOM for high-mobility devices. The remaining scatter of low-mobility devices with $\alpha_0\mu\tau$ in (a) and high-mobility devices with $\alpha_0\tau$ in (b) largely originates from devices with mobilities around the critical threshold mobility of $\mu_{crit} = 10^{-3}$ cm^2/(V s). The degree of scatter in the FOMs varies with the choice of threshold mobility. Figure S3 in the Supplemental Material additionally shows that the scatter increases if α_0 is omitted from the FOM expressions [25].

Note that our discussion refers to a fixed value of the electrical band gap E_g, which governs the recombination dynamics in the absorber and determines the theoretical efficiency limit [2]. Whereas the Shockley-Queisser (SQ) limit compares the attainable efficiency of absorbers with different band gaps, we assess how α_0, μ, and τ govern the solar-cell efficiency for a fixed E_g. For very high values of α_0, μ, and τ, the solar cell reaches the SQ efficiency limit at the given band gap. Obviously, the presented models are applicable to any value of E_g. Supplemental Fig. S2 [25] shows that different values of the electrical band gap lead to qualitatively similar results and that the same figures of merit presented herein are applicable [25].

In summary, the thin-film solar-cell efficiency correlates well to the $\alpha_0\mu\tau$ product as FOM in the low-mobility regime, where charge-carrier collection affects the device performance. In the high-mobility regime, the efficiency correlates well with a different FOM—the $\alpha_0\tau$ product. In this case, the efficiency is thus determined by absorption and recombination processes and not by transport anymore, since charge-carrier collection is saturated at the optimum value. The correlation between efficiency and $\alpha_0\tau$ product in the high-mobility regime confirms the analytical calculations for the infinite-mobility case in Fig. 3. The same moderate value of the critical mobility of $\mu_{crit} = 10^{-3}$ cm^2/(V s) above which charge collection does not further improve was recently estimated in a different approach by Firdaus *et al.* [5] for organic solar cells.

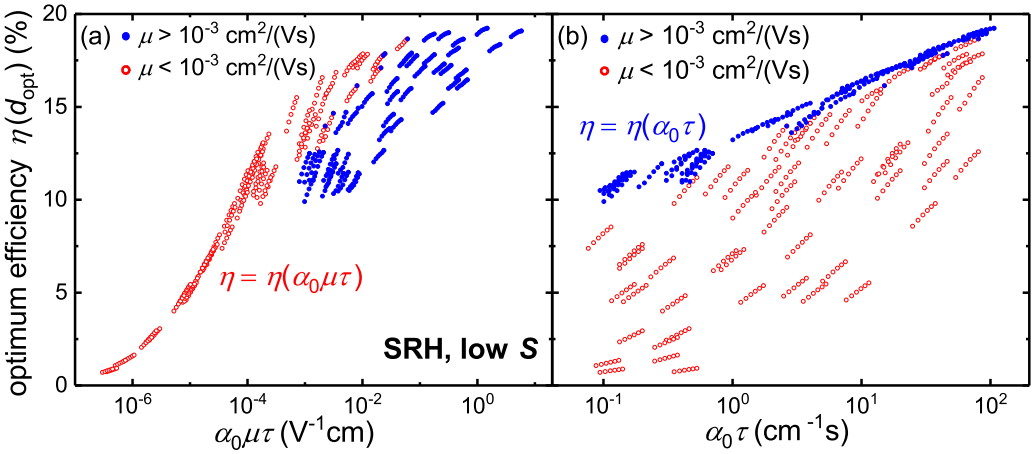

FIG. 4. Correlation between efficiency and different figures of merit (FOMs) based on α_0, μ, and τ for weak ($S = 10^{-3}$ cm/s) surface recombination and Shockley-Read-Hall bulk recombination. Each data point results from electrical drift-diffusion simulations [11,13,14] and optical simulations based on the transfer-matrix method [32] that accounts for interference in a representative layer stack. For different simulations, the electrical band gap is fixed, the standard absorption spectrum is scaled with a factor $c_\alpha \in [1, 1.5]$, and μ and τ are varied randomly over a wide range. For a given parameter set, the thickness is varied from 50 to 500 nm and the efficiency value is taken at the optimum thickness. (a), (b) contain the same dataset, which is separated into color-coded subsets of simulated devices with low- (red, open circle) and high- (blue, solid circle) mobility values, because the mobility regime largely determines which FOM is applicable. (a) The efficiency of low-μ dataset correlates well with $\alpha_0\mu\tau$, whereas in (b), the efficiency of the high-μ dataset correlates well with $\alpha_0\tau$, because the mobility becomes irrelevant once the collection is efficient and the efficiency value is taken at the optimum thickness d_{opt}.

V. RESULTS: INFLUENCE OF SURFACE RECOMBINATION

In Fig. 5, surface recombination, characterized by the surface-recombination velocity S, is non-negligible and eventually limits device performance for good bulk properties. The situation for the low mobilities is similar to the case of weak surface recombination and the efficiency depends on $\alpha_0\mu\tau$. The major difference to the low-S case in Fig. 4 is that the maximum efficiency $\eta(d_{\text{opt}})$ is capped at a significantly lower value which goes along with a different behavior of devices with high mobility. For low bulk recombination, the V_{oc} and therefore the efficiency is limited by recombination at the surface. Above a certain $\alpha_0\mu\tau$ value, the surface-recombination velocity thus determines the efficiency and higher values of $\alpha_0\mu\tau$ or $\alpha_0\tau$ are not beneficial. In fact, even a slight decrease in efficiency is observed for the highest $\alpha_0\mu\tau$ values in Fig. 5(a), because the mobility couples to the V_{oc} in the high-S case [24]: the time that charge carriers take to travel to the contacts influences the recombination rate at the surface. The impact of μ on V_{oc} might also explain why the scatter reduces for low mobilities, when the weights of α_0, μ, and τ are slightly varied and the mobility is emphasized as shown in Fig. S4(b) [25].

Figure 10 in Appendix B shows simulations for intermediate values for the surface-recombination velocity. A continuous trend between the low $S = 10^{-3}$ cm/s and high $S = 10^7$ cm/s cases discussed previously is observed. The

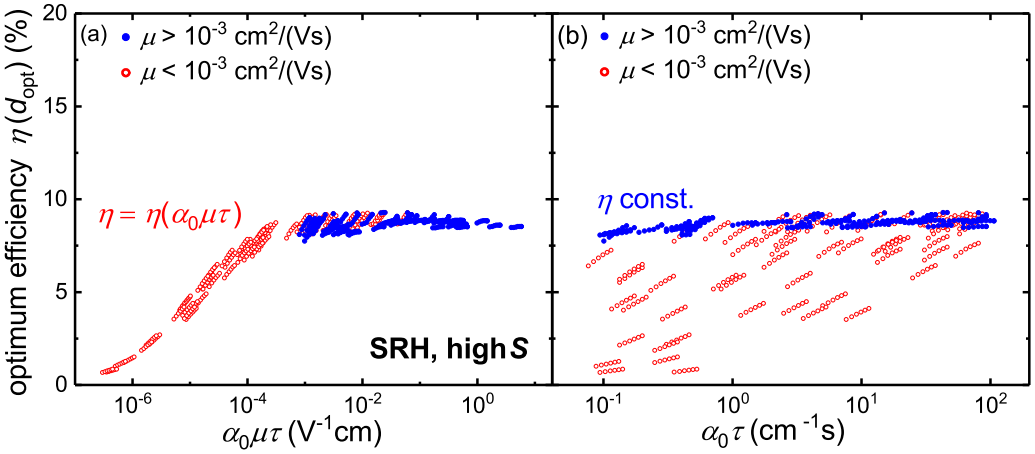

FIG. 5. Same type of plot as in Fig. 4, but for a dataset based on strong ($S = 10^7$ cm/s) surface recombination. (a) As in Fig. 4, the efficiency of the low-μ dataset correlates well with $\alpha_0\mu\tau$. (b) The efficiency of the high-μ dataset is independent of α_0, μ, and τ because the efficiency is solely governed by the strong surface recombination for good bulk properties.

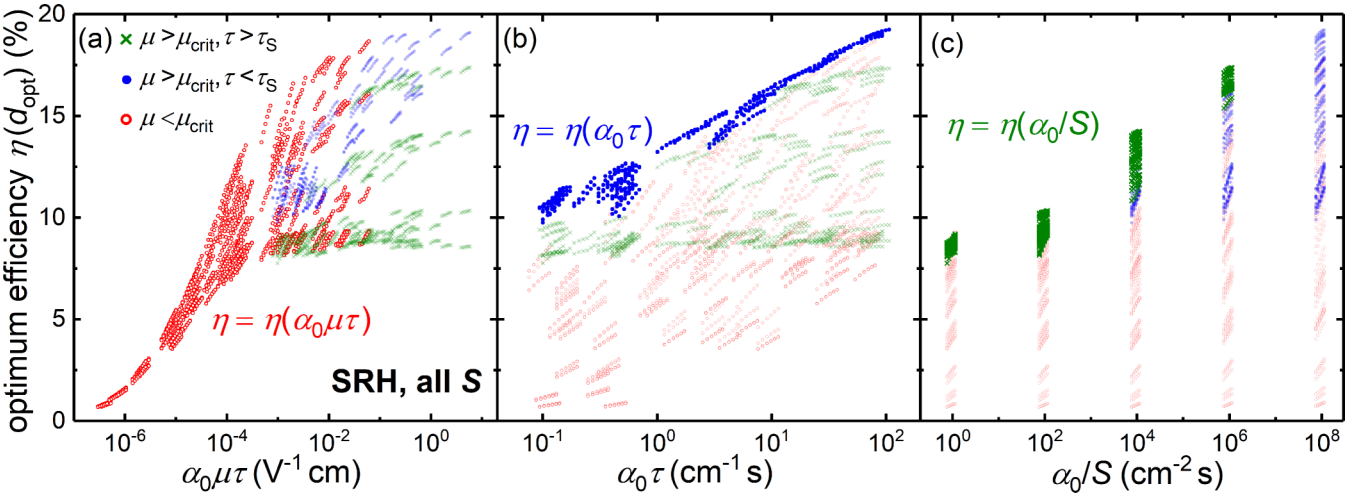

FIG. 6. FOMs accounting for variations in surface recombination velocity. Simultaneously considering surface-recombination velocities between $S = 10^{-3}$ cm/s and 10^5 cm/s leads to a new regime for the high-mobility case [$\mu > \mu_{crit} = 10^{-3}$ cm^2/(V s)]. The critical lifetime $\tau_S = 10^{-4.5} S^{-0.5} \sqrt{\text{cm s}}$ discriminates between regimes where bulk or surface recombination dominates. In the low-mobility regime (a) the $\alpha_0 \mu \tau$ product remains a meaningful FOM. For high mobilities and dominant bulk recombination (b) the $\alpha_0 \tau$ product is a good FOM. When surface recombination dominates (c) the α_0/S ratio as an additional FOM predicts the efficiency well.

efficiency is sensitive to changes in S between 10^{-3} cm/s and 10^5 cm/s. Figure 5, and Fig. 10 in Appendix B, show that for high mobilities a third regime exists, where surface recombination dominates over bulk recombination. Here, the $\alpha_0 \tau$ product is not a good FOM for all devices with high mobility as is explicitly shown in Fig. 11(b) in Appendix B. A third FOM for the efficiency describing high mobilities and dominant surface recombination should then contain the surface-recombination velocity S instead of the bulk lifetime τ. Figure 6 displays all data clouds for varying surface-recombination velocities between $S = 10^{-3}$ cm/s and $S = 10^5$ cm/s. The data are grouped into three different regimes with the low-mobility regime $\mu < \mu_{crit} = 10^{-3}$ cm^2/(V s) (red, open) defined as before. The inclusion of different values of surface recombination increases the scatter in the data towards higher values of $\alpha_0 \mu \tau$ since the interplay between charge collection, bulk, and surface recombination cannot be easily disentangled.

In order to find out whether certain subsets of the data follow a logical trend that cannot be observed from Fig. 6(a), we have to define additional categories. In addition to distinguishing two regimes for low and high mobilities, it is important to distinguish between situations where bulk or surface recombination dominates the total recombination rate. Therefore, the high-mobility regime $\mu > \mu_{crit}$ is further split up into two categories according to the values of bulk lifetime τ and surface-recombination velocity S. From the surface-recombination velocity, we can calculate a critical lifetime τ_S that distinguishes the two regimes. Since higher surface-recombination velocities cause charge carriers to recombine faster, τ_S should have a reciprocal relationship with S. In analogy to the choice of the critical mobility, the choice of τ_S results from minimizing the scatter in the two relevant regimes. We find the critical lifetime to be $\tau_S = 10^{-4.5} S^{-0.5} \sqrt{\text{cm s}}$. Our choice of τ_S is further rationalized in Appendix B. Note that certain alternative definitions for τ_S may produce similarly good results as shown in Fig. 12 in Appendix B. For short bulk lifetimes $\tau < \tau_S$ (blue, solid circle in Fig. 6) recombination in the bulk dominates and Fig. 6(b) shows that the $\alpha_0 \tau$ product remains a good FOM for the efficiency. For higher values of S the critical lifetime τ_S decreases. When surface recombination dominates for $\tau > \tau_S$ (green, cross), Fig. 6(c) shows the α_0/S ratio as a new FOM that governs the efficiency. Figure 11 in Appendix B gives an alternative representation of the scenario by unifying the two high-mobility cases through an effective lifetime defined as $\tau_{eff}^{-1} = \tau^{-1} + \tau_S^{-1}$. Then the $\alpha_0 \tau_{eff}$ product is a good FOM for the high-mobility case.

VI. APPLICATION: ORGANIC SOLAR CELLS

Most experimentally reported organic solar cells (OSCs), including almost all nonfullerene acceptor blends that represent today's most efficient OSCs, have an optimum thickness at the first absorption maximum around $d_{opt} \approx 100$ nm [33–39]. At larger thickness, poor charge-carrier collection in the cells typically results in a decrease in fill factor and thus efficiency [5,16,18,40]. Notable exceptions include certain fullerene-based OSCs that reach their optimum efficiency well above 100 nm thickness such as P3HT [41], PNTz4T [42], and PffBT4T [43], as well as a few nonfullerene acceptor-based OSCs that were shown to retain a relatively high fill factor at 200 nm, such as PTZ1:IDIC [44] and PBDB-TF:IT-4F [45]. At low absorber thickness, a considerable amount of incoming photons is not absorbed, leading to significant losses in the absorptance, external quantum efficiency, and short-circuit current density. Recently, an increased absorption strength has been demonstrated experimentally for certain polymers [26] and nonfullerene acceptors [27,38]. In the following, we assess the increase in efficiency that can be achieved for molecular materials with enhanced absorption. Generally, μ and τ vary over several orders of magnitude [18,39,46,47] between different materials, whereas α_0 only varies over roughly one order of magnitude as presented in Fig. 2. Nevertheless, for absorbers that reach intermediate efficiencies and a $\mu\tau$

product that does not enable very thick devices, an increase in α_0 may substantially increase the efficiency at the optimum thickness. We start our discussion by recapping differences in the recombination mechanism between organic and inorganic solar cells.

Inorganic semiconductor-based solar-cell materials are quite sensitive to deep localized states in the band gap of the semiconductor. This is due to the fact that nonradiative band to band transitions are quite unlikely due to the low phonon energies relative to the band gap and the strong dependence of multiphonon transitions on the number of phonons necessary for a single transition [48,49]. Localized states therefore strongly accelerate nonradiative transitions. The description of recombination using a Shockley-Read-Hall (SRH) lifetime τ, as has been done in this manuscript up to this point, is therefore representative for a wide range of inorganic solar cells. In organic solar cells, direct, bimolecular recombination between electrons and holes is highly relevant [12,39,50–54]. In such a recombination process, one electron and one hole come together at the donor-acceptor heterojunction to form a charge transfer state. This charge transfer state may then decay to the ground state nonradiatively without needing additional lower-lying electronic states in the band gap as in the case of inorganic solar cells. This pathway for recombination is enabled by the large vibrational energies of organic molecules, which are substantially higher than phonon energies in inorganic crystals [22,55]. Therefore, nonradiative recombination may dominate the total recombination rate even in the absence of deep defects. For such bimolecular recombination, charge-carrier lifetime becomes dependent on charge-carrier density, because the rate depends on the availability of both electrons and holes at the same place, and recombination is characterized by the bimolecular recombination coefficient k. The recombination rate is given by $R_{\mathrm{dir}} = knp$, with charge-carrier densities n and p, instead of $R_{\mathrm{SRH}} = n/\tau$ for monomolecular Shockley-Read-Hall recombination. Evidence for the presence of bimolecular recombination in organic solar cells is derived from the ideality factors of around 1 that are typically but not always found in organic solar cells [56–58]. These ideality factors of around 1 are substantially different from ideality factors of around 2 that would be expected for thin solar cells with nominally undoped absorber layers limited by recombination via deep defects. Hence, for the specific application of organic solar cells it makes sense to study the equivalent of Figs. 4 and 5 for the case of dominant bimolecular (direct) recombination. Drift-diffusion simulations of organic solar cells are based on the effective medium approach in which effective parameters (such as μ and k) are assigned to the organic absorber layer composed of a donor-acceptor bulk heterojunction. Although the microstructure of the blend film is neglected, this approach has been successfully applied to organic solar cells [5,11,12,59–61]. The resulting data in Fig. 7 behave very similarly to the data obtained for Shockley-Read-Hall recombination in Figs. 4 and 5 and the FOMs describing bimolecular recombination produce equally good results, in the limit of both slow and fast surface recombination. In the corresponding expressions for the bimolecular FOMs, $k^{-0.5}$ replaces the τ from the SRH case. Explicitly, the FOMs for bimolecular recombination read $\alpha_0\mu k^{-0.5}$ for the low-mobility case and $\mu k^{-0.5}$ for the high-mobility case—compared to $\alpha_0\mu\tau$ and $\alpha_0\tau$, respectively, for SRH recombination. Note that the different units of τ and k—stemming from the different recombination rates—cause the corresponding FOMs to have different units. The absolute values for the efficiency need to be understood in terms of the Shockley-Queisser efficiency for the assumed band gap of 0.9 eV. This means, even though reported experimental organic solar-cell efficiencies match the highest computed efficiencies in Fig. 7, the devices are likely still in the low-mobility regime as indicated by a low optimum thickness and fill factor.

From the data generated for Fig. 7, we calculate the gain in absorptance and efficiency for increased absorption strength. Figure 8(a) displays the maximum attainable short-circuit current density $J_{\mathrm{sc,max}}$, which is obtained for ideal charge-carrier collection at $V = 0$ V and thus reflects the absorptance. Since the optical model takes interference effects into account, maxima appear in the absorptance-thickness relation that translate to the displayed $J_{\mathrm{sc,max}}$. There is a notable difference in $J_{\mathrm{sc,max}}$ for different absorption strengths around the first absorption maximum. For thicker absorbers, this difference vanishes because $J_{\mathrm{sc,max}}$ saturates for all displayed absorption strengths. In quantitative terms, the attainable $J_{\mathrm{sc,max}}$ increases by around 15% at $d = 100$ nm for an increase by a factor of 1.5 in α_0 as can be seen from Fig. 8(b).

Figure 8(c) compares the resulting efficiencies for the case of a regular (standard spectrum α_{std}, blue, solid circle) and enhanced ($1.5\alpha_{\mathrm{std}}$, red, open circle) absorption strength in dependence on the $\mu k^{-0.5}$ product. As before, each device is evaluated at its individual optimum absorber thickness. See Fig. S6 in the Supplemental Material for further analysis of the optimum thickness [25]. The increase in efficiency with $\mu k^{-0.5}$ results from improved charge-carrier collection—just as for the corresponding $\mu\tau$ product for SRH recombination in Fig. 1. At any constant value of $\mu k^{-0.5}$, the efficiency of devices with enhanced absorption is clearly shifted upwards. Figure 8(d) further quantifies the gain in efficiency $\eta(c_\alpha = 1.5)/\eta(c_\alpha = 1) - 1$ when moving from regular to strong absorption. This gain tends towards zero for the highest $\mu k^{-0.5}$ values, where charge-carrier collection is perfectly efficient and the optimum thickness d_{opt} reaches several hundreds of nanometers as shown in Fig. S5 [25]. For such thick layers, the absorptance saturates for both regular and enhanced absorption strengths and the gain in absorptance in Fig. 8(b) vanishes, just as the gain in efficiency in Fig. 8(d). For lower $\mu k^{-0.5}$ values, the gain in efficiency is generally higher. The specific $\mu k^{-0.5}$ values at which the gain behavior changes coincide with jumps to a higher absorption maximum as indicated by the gray areas in Fig. 8(d) and shown in detail in Fig. S5 [25]. Generally, the optimum thickness of a regular absorbing blend jumps to the next higher absorption maximum at a lower $\mu k^{-0.5}$ value compared to a strongly absorbing blend. For example, for $\mu k^{-0.5}$ values in between the two gray regions, the regular absorbing blend has an optimum thickness around the second absorption maximum, whereas the strongly absorbing blend still performs best at a thickness around the first absorption maximum. Most importantly, for a range of relevant $\mu k^{-0.5}$ values that do not allow a jump to the second absorption maximum, a considerable gain in efficiency between 10% and almost 20% is reached.

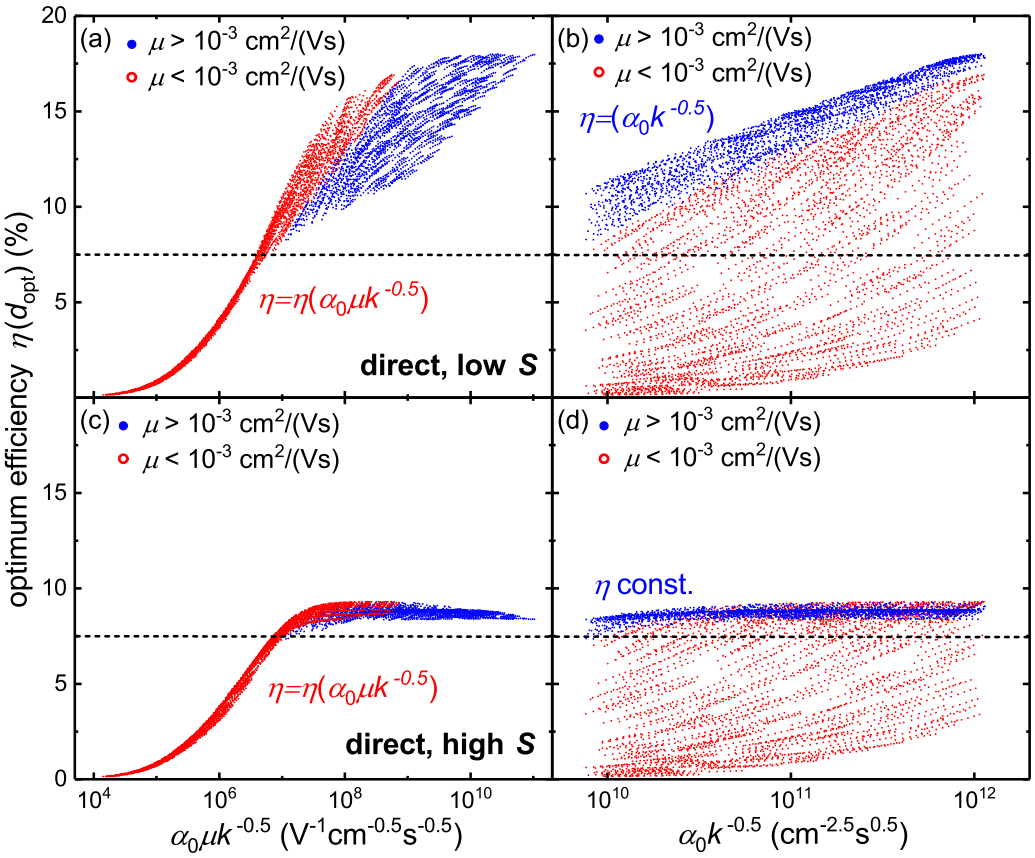

FIG. 7. Simulations for the case of bimolecular (direct) recombination characterized by the (direct) recombination coefficient k. (a), (b) weak surface recombination and (c), (d) strong surface recombination. The results qualitatively and quantitatively resemble those obtained for SRH recombination characterized by the lifetime τ in the corresponding Figs. 4 and 5. The FOMs for the (a), (c) low-mobility regime and (b), (d) high-mobility regime are modified to contain the recombination coefficient k instead of τ. The dashed lines indicate the transition towards a saturated efficiency for high surface-recombination velocities.

In summary, given that the optimum absorber thickness of many organic solar cells is at the first absorption maximum, an efficiency increase of around 15% seems realistic for an increase in the absorption strength by 50% ($c_\alpha = 1.5$). It is generally plausible that higher absorption strengths—leading to even larger gains in efficiency—could be reached once the parameter α_0 is in the focus of synthetic chemists who design new absorber materials. The absorption coefficient is related to the oscillator strength of the optical transitions in a semiconductor or molecule. The sum of the oscillator strength of different transitions cannot exceed the number of electrons in a given volume as defined by the Thomas-Reiche-Kuhn sum rule [26,62]. If one now adds up the oscillator strengths of highly absorbing molecules used for photovoltaics, Vezie *et al.* [26] found that the summed-up oscillator strength in the visible (where experimental data are readily available) amounts to only 10% of the number of electrons per volume indicating that a substantial fraction of absorption takes place outside the visible spectral region. Thus, it is at least conceivable that absorption could be further optimized by moving some optical transitions from the UV into spectral regions that are of interest for photovoltaics. Compared to most typical polymers, the increased absorption coefficient of certain novel small molecule acceptors in Fig. 2(b) is promising in that respect.

VII. SUMMARY AND DISCUSSION

The three material properties, absorption coefficient α, charge-carrier mobility μ, and charge-carrier lifetime τ (or recombination coefficient k), jointly determine the performance potential of any absorber material applied in a real-world solar cell. When good bulk properties of the absorber permit high solar-cell efficiency, the interface of the absorber to the contacts may ultimately limit the performance. Our findings provide a general understanding of the relative importance of these fundamental material and interface properties for the solar-cell efficiency. We found three different figures of merit (FOMs) describing different regimes of mobility, lifetime, and surface recombination. In the low-mobility regime, charge collection has a major influence on solar-cell efficiency which is then governed by the $\alpha_0\mu\tau$ product. In that case, α, μ, and τ are equally important for the efficiency, but experimental values of μ and τ cover a significantly wider range than α. Above a critical mobility of $\mu_{\mathrm{crit}} = 10^{-3}$ cm^2/(V s) charge collection is optimal and higher mobilities do not improve solar-cell performance. Only bulk and surface recombination determine the efficiency in addition to α. We observe the efficiency to change with surface-recombination velocity for values between $S = 10^{-3}$ cm/s and 10^5 cm/s. The maximum attainable efficiency doubles for the lowest S compared

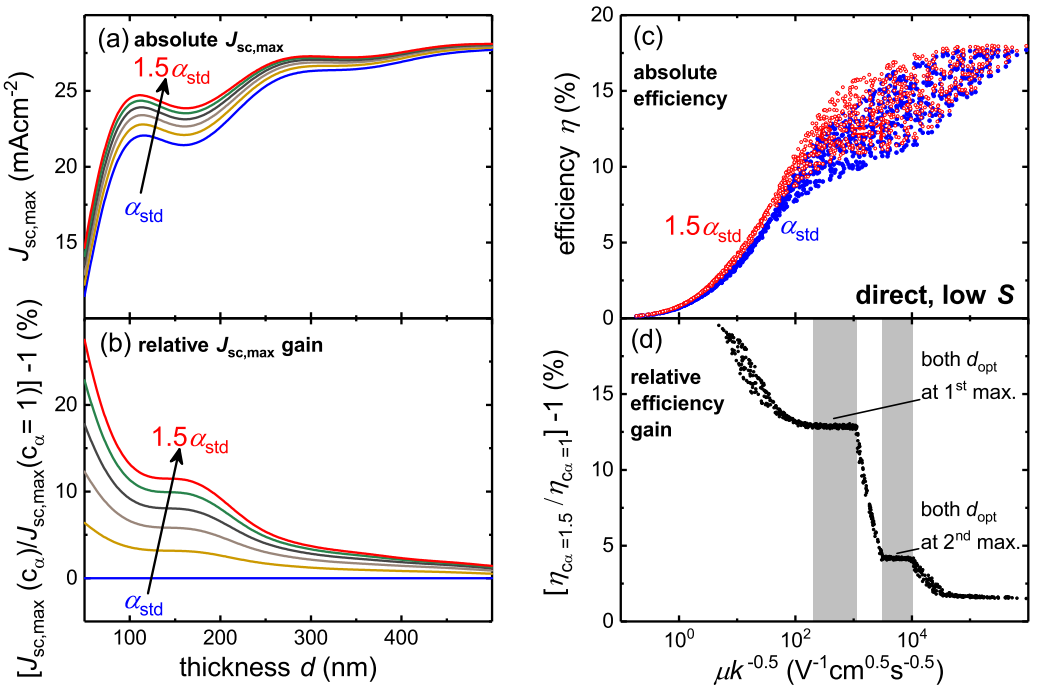

FIG. 8. Benefits of an increased absorption strength ($\alpha = c_\alpha \alpha_{std}$ with $c_\alpha \in [1, 1.5]$) based on a representative scenario for organic solar cells where a comparable tuning of α has been achieved [26]. (a) Maximum attainable short-circuit current density for ideal charge-carrier collection leading to (b) relative gains around 15% for thin absorber layers. At larger thickness, the absorptance tends to the same value for different absorption strengths and the attainable gain diminishes. The data in (a), (b) are only based on optical simulations. (c) Efficiency of the lowest ($c_\alpha = 1$, blue, solid circle) and highest ($c_\alpha = 1.5$, red, open circle) absorption strength simulated in Fig. 7 for bimolecular recombination and low surface-recombination, evaluated at the individually optimized thickness. (d) Relative efficiency increase for enhanced absorption $[\eta(d_{opt}, c_\alpha = 1.5)/\eta(d_{opt}, c_\alpha = 1)]$. Only devices with $d_{opt} > 50$ nm, which is the lowest simulated thickness, are included. The features of the data in (d) coincide with jumps to higher absorption maxima as is elaborated in Fig. S5 in the Supplemental Material [25]. The gain attained by stronger absorption depends heavily on $\mu k^{-0.5}$ and reaches a value of around 15% for $\mu k^{-0.5}$ values that are associated with a typical optimum thickness for organic solar cells of about 100 nm at the first absorption maximum.

to the highest S considered. In the high-mobility case, the surface-recombination velocity defines a critical lifetime $\tau_S = 10^{-4.5} S^{-0.5} \sqrt{\text{cm s}}$. For smaller bulk lifetimes, recombination in the bulk dominates and the efficiency is governed by the $\alpha_0 \tau$ product. For longer bulk lifetimes the α_0/S ratio governs solar-cell efficiency and recombination at the surface poses the ultimate limit to this efficiency until it reaches the Shockley-Queisser limit. Importantly, the absorption coefficient is relevant in all three regimes. All our results apply to thin-film solar cells with uniform electric field and optimized absorber thickness. The latter is easily obtained in simulations and experiments by simply preparing a series of solar cells with varying absorber thickness and selecting the thickness that performs best.

For the case of organic solar cells whose $\mu\tau$ product often yields an optimum thickness at the first absorption maximum around 100 nm, a moderate increase in absorption coefficient by a factor of 1.5 brings an increase in relative efficiency of approximately 15%. Such enhanced absorption has been demonstrated experimentally and offers a route to overcome today's efficiency limits as organic solar cells typically operate in the regime where the $\alpha_0 \mu\tau$ product is the relevant figure of merit. The tailoring of the absorption strength is thus another relevant optimization parameter in the design of organic absorber materials. For the same reason absolute (not normalized) absorption values should be included in reports.

Our findings can be used to compare different absorber technologies to each other and to distinguish the causes of deviation from the Shockley-Queisser efficiency limit. By determining α, μ, and τ of the absorber film, a material's efficiency potential can be estimated without having to optimize the full device structure. Our results are thus valuable for material screening of organic or inorganic absorbers by means of both experimental material synthesis and computational material screening. Eventually, knowing the relative importance of the three material quantities α, μ, and τ for the solar-cell efficiency enables a more targeted search for suitable absorber materials.

ACKNOWLEDGMENTS

P.K. acknowledges the support by the Global Challenges Research Fund (GCRF) through Science & Technology Facilities Council (STFC), Grant No. ST/R002754/1: Synchrotron Techniques for African Research and Technology (START). T.K. and U.R. acknowledge support from the Helmholtz Association for funding via the PEROSEED project. J.N. thanks the UK Engineering and Physical Sciences Research Council (Grant No. EP/P005543/1) and the European Research Council (Grant Agreement No. 742708) for funding.

There are no conflicts of interest to declare.

APPENDIX A: METHODS

1. Optical simulations

The optical simulations in Figs. 3–5 are based on the data of a DPPTTT:PCBM bulk heterojunction, that reflects typical organic absorber blends. The mixed donor-acceptor blend has a broader absorption spectrum but lower κ_0 compared to the pure polymer data shown in Fig. 2. Specifically, we use the absorption spectrum of the high molecular weight DPPTTT:PCBM blend divided by a factor of 1.5 as the standard spectrum α_{std}, as shown in Fig. 9. The standard spectrum is then scaled ($\alpha = c_\alpha \alpha_{\mathrm{std}}$) by a varying factor c_α in the different simulations. To characterize the absorption strength we use α_0, which then also enters the defined figures of merit. Since c_α scales the whole spectrum, it does so with α_0 as well. The illustrative calculations for the infinite-mobility limit in Fig. 3 apply a simple Lambert-Beer model without interference and scale the standard spectrum between $c_\alpha \in [0.5, 2]$. For Figs. 4 and 5, interference is taken into account and the spectrum is scaled by a factor between $c_\alpha \in [1, 1.5]$, which reflects the experimentally achieved tuning of the DPPTTT:PCBM blend's absorption strength in Ref. [26] as can be seen from Fig. 9. Any change in reflectance caused by a change in refractive index accompanying the variation of the absorption coefficient is neglected. The optical position- and wavelength-dependent generation profiles are computed with the transfer-matrix method [32] for a representative *n-i-p* OSC stack with flat interfaces consisting of glass/ITO (150 nm)/ZnO (40 nm)/absorber blend/MoO_3 (10 nm)/Ag (100 nm). The absorption profiles obtained from optical simulations directly yield the generation profiles of free charge carriers—implying that any loss in exciton dissociation is neglected. In particular, exciton dissociation is assumed voltage independent and independent of α_0, μ, or k (or τ).

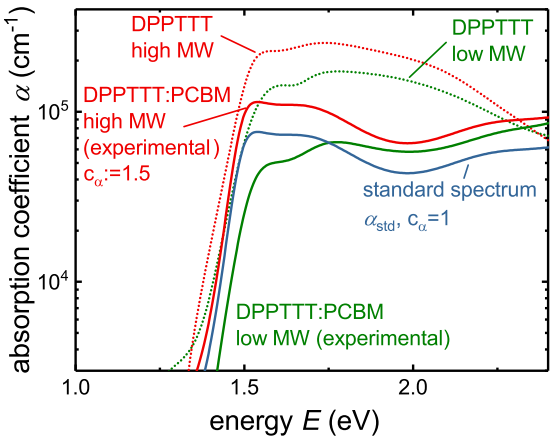

FIG. 9. Absorption spectra of DPPTTT and DPPTTT:PCBM blends. The high-MW DPPTTT:PCBM blend spectrum, scaled by different factors, serves as input for the optical simulations for Figs. 3–5. The standard spectrum α_{std}, assigned with $c_\alpha = 1$, results from dividing the experimentally recorded high-MW DPPTTT:PCBM spectrum by 1.5 and reflects the absorption strength of typical OSC blends. The original experimental data are recovered for $c_\alpha = 1.5$. By simply scaling a defined spectrum, we focus on the effect of absorption strength and avoid any effects arising from different spectral shapes if, e.g., the experimentally recorded high- and low-MW blends were used in the simulations.

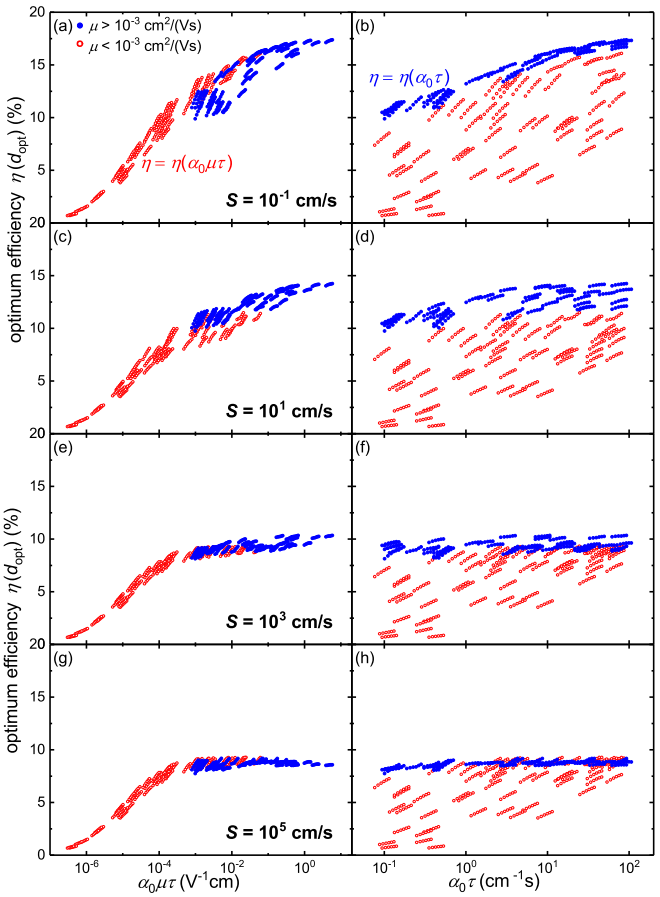

FIG. 10. Impact of surface recombination on maximum attainable efficiency for trap-assisted recombination in the bulk. The trend between the high $S = 10^{-3}$ cm/s and low $S = 10^7$ cm/s cases discussed in the main paper is continuous. No change between $S = 10^5$ cm/s and $S = 10^7$ cm/s is observed. The $\alpha_0 \mu\tau$ product is a good figure of merit for the low-mobility case. For the high-mobility case, the $\alpha_0 \tau$ product loses its predictive power on the efficiency as recombination at the surface, characterized by S, becomes increasingly dominant over bulk recombination, characterized by τ.

2. High-mobility limit

In the scenario of Fig. 3, charge-carrier collection is 100% efficient and no surface recombination is considered. In the absence of collection losses, an explicit expression for the current-voltage characteristic is derived following the models presented in Refs. [1,29], which then directly yields the solar-cell efficiency. The electrical band gap is fixed at $E_g = 1.6$ eV. The total current density J is given by the sum

$$J = -J_{\mathrm{sc}} + J_{\mathrm{rad}} + J_{\mathrm{non-rad}} \tag{A1}$$

of the short-circuit current density J_{sc}, which equals the photocurrent for ideal collection, the radiative recombination current density J_{rad}, and the nonradiative recombination current density J_{nonrad}. The first term is generally given by

$$J_{\mathrm{sc}} = q \int_0^\infty Q_e \phi_{\mathrm{sun}}\, dE, \tag{A2}$$

TABLE I. Standard input parameters for the optical and drift-diffusion simulations in Figs. 4–8 and 10–12, and Figs. S2–S6 in the Supplemental Material [25], where the optimum absorber thickness yielding the highest efficiency is chosen. Appendix section A 1 and A 3 rationalize the choice of parameters.

Parameter		Value	Unit
Thickness	d	50–500	nm
Mobility	$\mu_{e,h}$	10^{-6}–10^{-1}	$cm^2(V\,s)^{-1}$
Direct recombination coefficient	k	10^{-10}–10^{-14}	$cm^3\,s^{-1}$
SRH lifetime	τ	10^{-6}–10^{-3}	S
Scaling factor ($\alpha = c_\alpha \alpha_{std}$)	c_α	1–1.5	–
Effective band gap	E_g	0.9	eV
Schottky barriers	φ	0.1	eV
Minority surface recombination velocity	S_{min}	10^{-3}–10^{7}	$cm\,s^{-1}$
Majority surface recombination velocity	S_{maj}	10^{9}	$cm\,s^{-1}$
Dielectric constant	ϵ_r	3.5	–
Effective DOS	$N_{c,v}$	10^{19}	cm^{-3}

with the solar AM1.5 spectrum and the quantum efficiency $Q_e = a(E)$, which equals the absorptance for ideal collection. A suitable optical model is required for the absorptance. Here, we choose Lambertian light trapping [31] without interference.

The radiative current follows,

$$J_{rad} = J_{0,rad}\left(e^{\frac{qV}{k_b T}} - 1\right), \tag{A3}$$

where the radiative saturation current density is obtained from the blackbody emission spectrum ϕ_{bb} of the solar cell and by again equating $Q_e = a(E)$:

$$J_{0,rad} = \int_0^\infty q\, a \phi_{bb}(T = 300\ \mathrm{K})\, dE. \tag{A4}$$

For the nonradiative contribution to the recombination current, we assume Shockley-Read-Hall recombination as the dominant mechanism. For an intrinsic—and thus fully depleted—absorber layer, electron and hole concentrations are approximately equal ($n \approx p$) and the solar cell operates in the high injection limit. For equal charge-carrier lifetimes $\tau_n = \tau_p = \tau$, the saturation current density is then given by

$$J_{0,nonrad} = qd\frac{\sqrt{N_c N_v}}{2\tau}\, e^{-\frac{E_g}{2k_b T}}, \tag{A5}$$

where d is the absorber layer thickness and $N_{c,v}$ are the effective density of states of the conduction and valence band. The nonradiative current density is

$$J_{nonrad} = J_{0,nonrad}\left(e^{\frac{qV}{2k_b T}} - 1\right). \tag{A6}$$

Finally, by substituting Eqs. (A2)–(A6) into (A1), the full J-V characteristic of the solar cell is obtained and the power $P = JV$ and efficiency,

$$\eta = \frac{\max(P)}{\int_0^\infty E\,\Phi_{sun}(E)dE}, \tag{A7}$$

of the device are obtained.

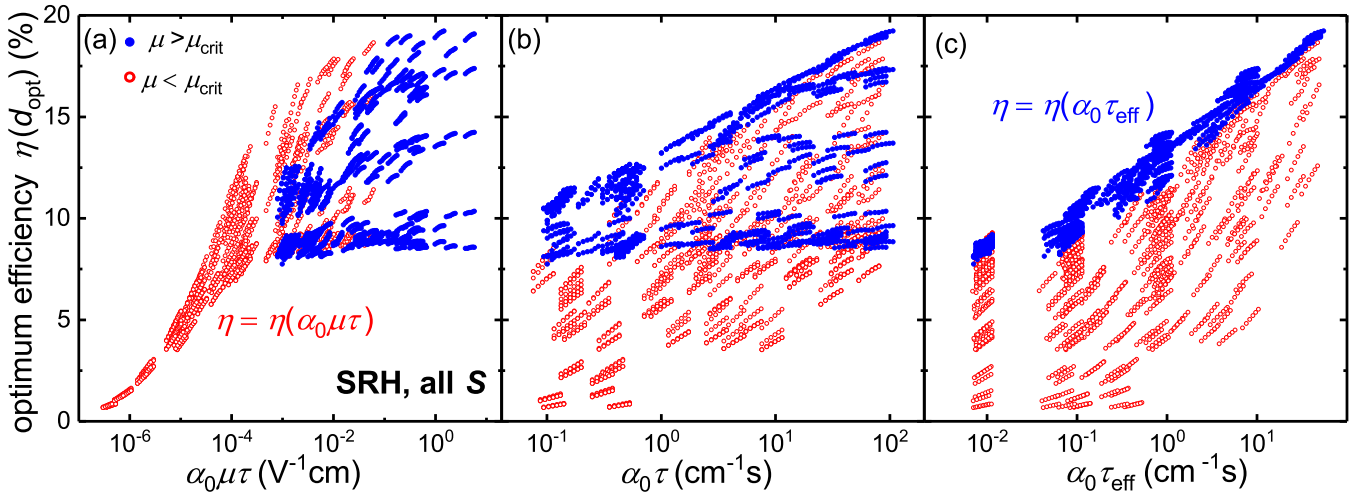

FIG. 11. Clouds including all data shown in Figs. 4 and 10 with surface-recombination velocities between $S = 10^{-3}$ cm/s and 10^5 cm/s. (a) Surface recombination also affects the low-mobility regime $\mu < \mu_{crit} = 10^{-3}$ $cm^2/(V\,s)$ and leads to increased scatter in the data. (b) The $\alpha_0\tau$–product is not a good FOM for the efficiency when different degrees of surface recombination are considered. (c) Alternatively to splitting the high-mobility regime in cases with dominating bulk or surface recombination as done in Fig. 6, an effective lifetime can be defined as $\tau_{eff}^{-1} = \tau^{-1} + \tau_S^{-1}$ with the critical lifetime $\tau_S = 10^{-4.5} S^{-0.5} \sqrt{cm\,s}$ as defined in the main text. The $\alpha_0\tau_{eff}$–product is again a good FOM for the high-mobility regime.

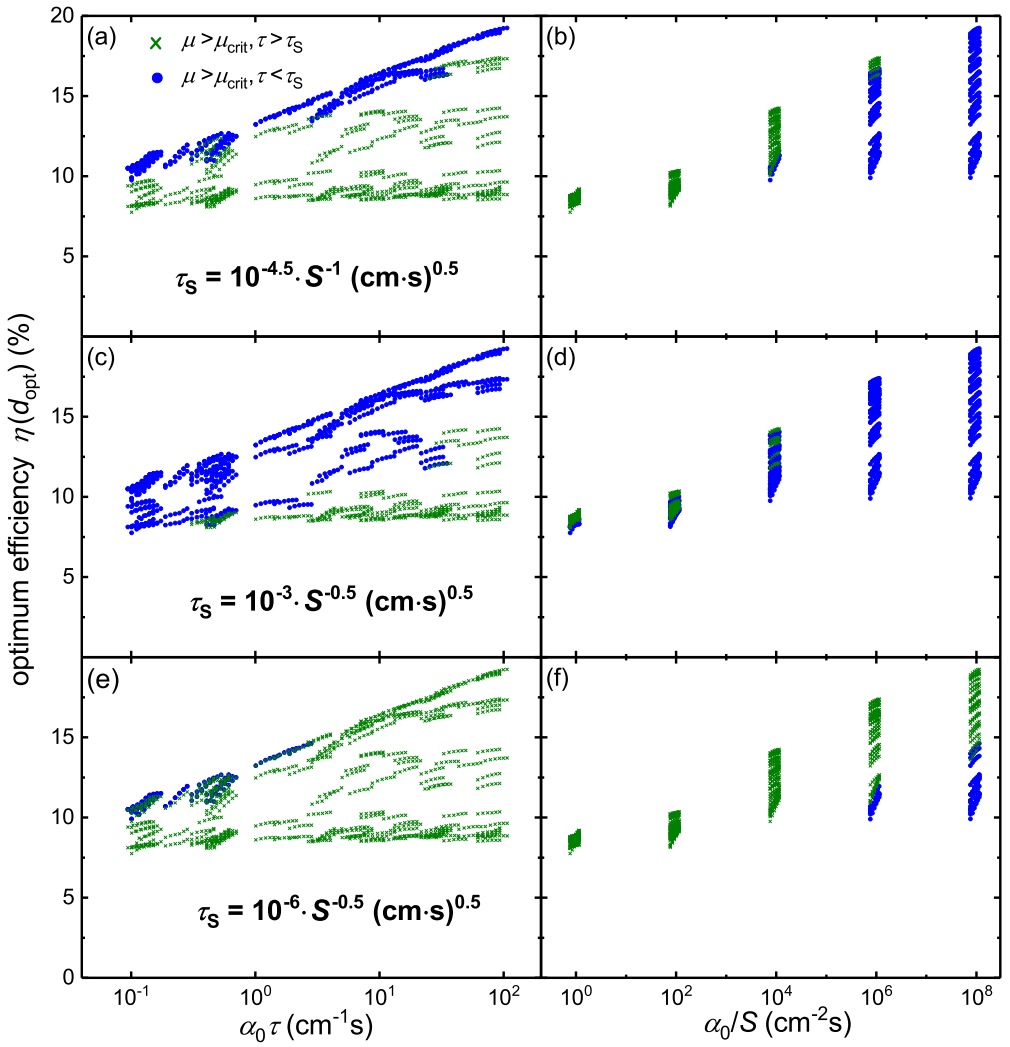

FIG. 12. Choice of critical lifetime τ_S that separates the two high-mobility regimes. By changing the proportionality from $\tau_S \sim S^{-0.5}$ (shown in the main part) to $\tau_S \sim S^{-1}$ in (a), (b), similarly good results are obtained. However, when the factor in the expression for τ_S is varied from $10^{-4.5}$ to 10^{-3} in (c), (d) or 10^{-6} in (e), (f), the scatter increases and correlations become significantly worse. Panels (a), (c), (e) show correlations to the $\alpha_0\tau$ product and panels (b), (d), (f) show correlations to the α_0/S ratio. To simplify the plots, data points for the low-mobility case $\mu < \mu_{crit}$ are not displayed.

3. Numerical simulations to include collection losses

To account for collection losses and the complexity introduced by surface recombination, we apply numerical drift-diffusion simulations [11,13–15,63] to compute current density-voltage (J-V) curves that yield the solar-cell efficiency. Electrical simulations are done with Advanced Semiconductor Analysis [64] (ASA). Motivated by the relatively low V_{oc} reached for DPPTTT-based solar cells in Ref. [26], the electrical band gap of the effective medium is fixed at $E_g = 0.9$ eV, which is likely to reflect the charge transfer state energy, with Schottky barriers of 0.1 eV at each contact. Two different cases of low ($S = 10^{-3}$ cm/s) and high ($S = 10^7$ cm/s) minority carrier surface-recombination velocity are studied. Surface recombination is negligible in the low-S case, which is thus close to the situation in Figs. 1 and 3. In a similar approach to Ref. [40] and our previous study on the fill factor of thin-film solar cells [18], the simulation input parameters μ and τ or k are chosen at random from a wide parameter range and we create large datasets covering a wide parameter space. The ranges of μ, τ, and k values in previous ensemble simulations of organic solar cells [18,40,60] are based on reported experimental results [50,52,65]. Here, we extend the parameter ranges to cover inorganic solar cells and future, better-performing organic solar cells. For a given set of parameters the absorber thickness is varied between 50 and 500 nm and the optimum thickness and corresponding highest efficiency is extracted. The simulation parameters are listed in Table I. The mobility of electrons and holes are set to the same value and no doping is included leading to a fully depleted device architecture with homogeneous electric field across the absorber layer. Either a bimolecular (direct) or a monomolecular (trap-assisted) Shockley-Read-Hall (SRH) recombination model—characterized by k and τ, respectively—is considered. In particular, traps are neglected in the bimolecular case that serves to represent organic solar cells. Note that in certain organic material systems, trap-assisted recombination is non-negligible [66,67].

4. Accuracy of simulations

The applied numerical simulations solve coupled partial differential equations, given by the drift-diffusion model for solar cells, with high accuracy [14]. The ASA [64] software used in this work uses the Gummel method for two iterations and then switches to the Newton method with a maximum of 40 iterations for each bias voltage point. No damping is applied for the Poisson equation and corrections that would result in negative concentrations are clipped for the continuity equations.

The drift-diffusion model generally well describes the behavior of thin-film solar cells such as organic solar cells [14,40,63]. One issue in comparison with experiments is the accurate experimental determination of material parameters such as surface-recombination velocity, lifetime, or mobility [68–72]. However, by varying almost all of the material parameters—including mobility, lifetime, absorption coefficient, surface-recombination velocity, and band gap—over a wide range, the relevant experimental parameter ranges are most likely covered. See Appendix B for further discussion on the influence of surface-recombination velocity and Fig. S2 in the Supplemental Material for the band gap [25].

APPENDIX B: INFLUENCE OF SURFACE RECOMBINATION

Surface recombination velocity as limiting factor. Figure 10 shows the impact of surface recombination on the maximum attainable efficiency for various values of the minority surface recombination velocity S. Intermediate cases of the low S and high S case in the main part of the paper are presented and show a continuous trend. Figure 11 introduces an effective lifetime $\tau_{\text{eff}}^{-1} = \tau^{-1} + \tau_s^{-1}$ which allows to treat the high mobility case as a single case even if the data include different values of surface recombination velocities.

Choice of τ_S. As discussed in the main part of this work, bulk recombination dominates for bulk lifetimes $\tau < \tau_S$ (blue) with the $\alpha_0\tau$ product as a good FOM. Surface recombination dominates for bulk lifetimes $\tau > \tau_S$ (green) with the α_0/S ratio as a good FOM. The semiheuristic choice for $\tau_S = 10^{-4.5} S^{-0.5} \sqrt{\text{cm s}}$ in the main part is rationalized in the following: The critical lifetime τ_S is governed by the value of the surface-recombination velocity S to which it should have a reciprocal relationship since a higher surface-recombination velocity causes charge carriers to recombine faster. As demonstrated in this manuscript, bulk and surface recombination compete over the investigated parameter range for bulk SRH lifetimes (between $\tau = 10^{-6}$ s and 10^{-3} s) and surface-recombination velocities (between $S = 10^{-3}$ cm/s and 10^{5} cm/s). Consequently, we map the values of surface-recombination velocities on the range of SRH lifetimes. Since τ covers four orders of magnitude and S covers eight orders of magnitude, we choose $\tau_S \sim S^{-0.5}$. In order to map the range of S values on the range of τ values an additional factor of $10^{-4.5}$ is needed. Figure 6 shows that this rationale for the choice of τ_S produces good correlations of the efficiency with the corresponding FOMs in Figs. 6(b) and 6(c). However, it cannot be expected that such a semiheuristic approach in stipulating a critical lifetime τ_S provides a unique definition and different choices for τ_S may provide similarly good results as shown in Fig. 12.

[1] T. Kirchartz and U. Rau, What makes a good solar cell? Adv. Energy Mater. **8**, 1703385 (2018).

[2] W. Shockley and H. J. Queisser, Detailed balance limit of efficiency of p-n junction solar cells, J. Appl. Phys. **32**, 510 (1961).

[3] A. Polman, M. Knight, E. C. Garnett, B. Ehrler, and W. C. Sinke, Photovoltaic materials: Present efficiencies and future challenges, Science **352**, 4424 (2016).

[4] J. Mattheis, J. H. Werner, and U. Rau, Finite mobility effects on the radiative efficiency limit of *pn*-junction solar cells, Phys. Rev. B **77**,085203 (2008).

[5] Y. Firdaus, V. M. L. Corre, J. I. Khan, Z. Kan, F. Laquai, P. M. Beaujuge, and T. D. Anthopoulos, Key parameters requirements for non-fullerene-based organic solar cells with power conversion efficiency greater >20%, Adv. Sci. **6**, 1802028 (2019).

[6] J. H. Reynolds and A. Meulenberg, Measurement of diffusion length in solar cells, J. Appl. Phys. **45**, 2582 (1974).

[7] N. D. Arora, S. G. Chamberlain, and D. J. Roulston, Diffusion length determination inp-njunction diodes and solar cells, Appl. Phys. Lett. **37**, 325 (1980).

[8] A. M. Goodman, A Method for the measurement of short minority carrier diffusion lengths in semiconductors, J. Appl. Phys. **32**, 2550 (1961).

[9] E. D. Stokes and T. L. Chu, Diffusion lengths in solar cells from short-circuit current measurements, Appl. Phys. Lett. **30**, 425 (1977).

[10] R. S. Crandall, Transport in hydrogenated amorphous silicon *p-i-n* solar cells, J. Appl. Phys. **53**, 3350 (1982).

[11] T. Kirchartz and J. Nelson, Device modelling of organic bulk heterojunction solar cells, Top. Curr. Chem. **352**, 279 (2014).

[12] L. J. A. Koster, E. C. P. Smits, V. D. Mihailetchi, and P. W. M. Blom, Device model for the operation of polymer/fullerene bulk heterojunction solar cells, Phys. Rev. B **72**, 085205 (2005).

[13] J. Nelson, *The Physics of Solar Cells* (World Scientific Publishing Company, Singapore, 2003).

[14] B. E. Pieters, K. Decock, M. Burgelman, R. Stangl, and T. Kirchartz, One-dimensional electro-optical simulations of thin-film solar cells, in *Advanced Characterization Techniques For Thin Film Solar Cells*, edited by D. Abou-Ras, T. Kirchartz, and U. Rau (Wiley, New York, 2016), pp. 633–657.

[15] S. Selberherr, *Analysis and Simulation of Semiconductor Devices* (Springer, Berlin, 2012).

[16] T. Kirchartz, T. Agostinelli, M. Campoy-Quiles, W. Gong, and J. Nelson, Understanding the thickness-dependent performance of organic bulk heterojunction solar cells: The influence of mobility, lifetime, and space charge, J. Phys. Chem. Lett. **3**, 3470 (2012).

[17] T. Kirchartz, J. Bisquert, I. Mora-Sero, and G. Garcia-Belmonte, Classification of solar cells according to mechanisms of charge separation and charge collection, Phys. Chem. Chem. Phys. **17**, 4007 (2015).

[18] P. Kaienburg, U. Rau, and T. Kirchartz, Extracting information about the electronic quality of Organic solar-cell absorbers from fill factor and thickness, Phys. Rev. Appl. **6**, 24001 (2016).

[19] M. A. Green, Accuracy of analytical expressions for solar cell fill factors, Sol. Cells **7**, 337 (1982).

[20] M. A. Green, Solar cell fill factors: General graph and empirical expressions, Solid-State Electron. **24**, 788 (1981).

[21] W. Tress, Perovskite solar cells on the way to their radiative efficiency limit—insights into a success story of high open-circuit voltage and low recombination, Adv. Energy Mater. **7**, 1602358 (2017).

[22] T. Kirchartz, T. Markvart, U. Rau, and D. A. Egger, Impact of small phonon energies on the charge-carrier lifetimes in metal-halide perovskites, J. Phys. Chem. Lett. **9**, 939 (2018).

[23] T. Kirchartz, L. Krückemeier, and E. L. Unger, Research update: Recombination and open-circuit voltage in lead-halide perovskites, APL Mater. **6**, 100702 (2018).

[24] O. J. Sandberg, A. Sundqvist, M. Nyman, and R. Österbacka, Relating charge transport, contact properties, and recombination to open-circuit voltage in sandwich-type thin-film solar cells, Phys. Rev. Appl. **5**, 044005 (2016).

[25] See Supplemental Material at http://link.aps.org/supplemental/10.1103/PhysRevResearch.2.023109 for absorption spectra of organic absorbers, scatter plots for modified FOMs with optimized weights, the influence of the band gap, and details for the case of bimolecular recombination.

[26] M. S. Vezie, S. Few, I. Meager, G. Pieridou, B. Dörling, R. S. Ashraf, A. R. Goñi, H. Bronstein, I. McCulloch, S. C. Hayes, M. Campoy-Quiles, and J. Nelson, Exploring the origin of high optical absorption in conjugated polymers, Nat. Mater. **15**, 746 (2016).

[27] L. Krückemeier, P. Kaienburg, J. Flohre, K. Bittkau, I. Zonno, B. Krogmeier, and T. Kirchartz, Developing design criteria for organic solar cells using well-absorbing non-fullerene acceptors, Commun. Phys. **1**, 27 (2018).

[28] P. Kaienburg, B. Klingebiel, and T. Kirchartz, Spin-coated planar Sb_2S_3 hybrid solar cells Approaching 5% efficiency, Beilstein J. Nanotechnol. **9**, 2114 (2018).

[29] B. Blank, T. Kirchartz, S. Lany, and U. Rau, Selection metric for photovoltaic materials screening based on detailed-balance analysis, Phys. Rev. Appl. **8**, 024032 (2017).

[30] R. Brendel and H. J. Queisser, On the thickness dependence of open circuit voltages of p-n junction solar cells, Sol. Energy Mater. Sol. Cells **29**, 397 (1993).

[31] M. A. Green, Lambertian light trapping in textured solar cells and light-emitting diodes: Analytical solutions, Prog Photovoltaics **10**, 235 (2002).

[32] G. F. Burkhard, E. T. Hoke, and M. D. McGehee, Accounting for interference, scattering, and electrode absorption to make accurate internal quantum efficiency measurements in organic and other thin solar cells, Adv. Mater. **22**, 3293 (2010).

[33] Z. He, C. Zhong, S. Su, M. Xu, H. Wu, and Y. Cao, Enhanced power-conversion efficiency in polymer solar cells using an inverted device structure, Nat. Photonics **6**, 593 (2012).

[34] S. H. Park, A. Roy, S. Beaupré, S. Cho, N. Coates, J. S. Moon, D. Moses, M. Leclerc, K. Lee, and A. J. Heeger, Bulk heterojunction solar cells with internal quantum efficiency approaching 100%, Nat. Photonics **3**, 297 (2009).

[35] S. E. Shaheen, C. J. Brabec, N. S. Sariciftci, F. Padinger, T. Fromherz, and J. C. Hummelen, 2.5% efficient organic plastic solar cells, Appl. Phys. Lett. **78**, 841 (2001).

[36] W. Zhao, S. Li, H. Yao, S. Zhang, Y. Zhang, B. Yang, and J. Hou, Molecular optimization enables over 13% efficiency in organic solar cells, J. Am. Chem. Soc. **139**, 7148 (2017).

[37] H. Li, Z. Xiao, L. Ding, and J. Wang, Thermostable single-junction organic solar cells with a power conversion efficiency of 14.62%, Sci. Bull. **63**, 340 (2018).

[38] D. Baran, R. S. Ashraf, D. A. Hanifi, M. Abdelsamie, N. Gasparini, J. A. Röhr, S. Holliday, A. Wadsworth, S. Lockett, M. Neophytou, C. J. M. Emmott, J. Nelson, C. J. Brabec, A. Amassian, A. Salleo, T. Kirchartz, J. R. Durrant, and I. McCulloch, Reducing the efficiency–stability–cost gap of organic photovoltaics with highly efficient and stable small molecule acceptor ternary solar cells, Nat. Mater. **16**, 363 (2016).

[39] T. Kirchartz, P. Kaienburg, and D. Baran, Figures of merit guiding research on organic solar cells, J. Phys. Chem. C **122**, 5829 (2018).

[40] D. Bartesaghi, I. del Carmen Pérez, J. Kniepert, S. Roland, M. Turbiez, D. Neher, and L. J. A. Koster, Competition between recombination and extraction of free charges determines the fill factor of organic solar cells, Nat. Commun. **6**, 7083 (2015).

[41] G. Li, V. Shrotriya, J. Huang, Y. Yao, T. Moriarty, K. Emery, and Y. Yang, High-efficiency solution processable polymer photovoltaic cells by self-organization of polymer blends, Nat. Mater. **4**, 864 (2005).

[42] V. Vohra, K. Kawashima, T. Kakara, T. Koganezawa, I. Osaka, K. Takimiya, and H. Murata, Efficient inverted polymer solar cells employing favourable molecular orientation, Nat. Photonics **9**, 403 (2015).

[43] J. Zhao, Y. Li, G. Yang, K. Jiang, H. Lin, H. Ade, W. Ma, and H. Yan, Efficient organic solar cells processed from hydrocarbon solvents, Nat. Energy **1**, 15027 (2016).

[44] B. Guo, W. Li, X. Guo, X. Meng, W. Ma, M. Zhang, and Y. Li, High efficiency nonfullerene polymer solar cells with thick active layer and large area, Adv. Mater. **29**, 1702291 (2017).

[45] Z. Zheng, Q. Hu, S. Zhang, D. Zhang, J. Wang, S. Xie, R. Wang, Y. Qin, W. Li, L. Hong, N. Liang, F. Liu, Y. Zhang, Z. Wei, Z. Tang, T. P. Russell, J. Hou, and H. Zhou, A highly efficient non-fullerene organic solar cell with a fill factor over 0.80 enabled by a fine-tuned hole-transporting layer, Adv. Mater. **30**, 1801801 (2018).

[46] R. S. Crandall and I. Balberg, Mobility-lifetime products in hydrogenated amorphous silicon, Appl. Phys. Lett. **58**, 508 (1991).

[47] R. Brüggemann, Steady-state photocarrier grating method, Adv. Charact. Tech. Thin Film Sol. Cells **1**, 163 (2016).

[48] T. Markvart, Semiclassical theory of non-radiative transitions, J. Phys. C: Solid State Phys. **14**, L895 (1981).

[49] B. K. Ridley, On the multiphonon capture rate in semiconductors, Solid-State Electron. **21**, 1319 (1978).

[50] D. Credgington, F. C. Jamieson, B. Walker, T.-Q. Nguyen, and J. R. Durrant, Quantification of geminate and non-geminate recombination losses within a solution-processed

small-molecule bulk heterojunction solar cell, Adv. Mater. **24**, 2135 (2012).

[51] L. J. A. Koster, V. D. Mihailetchi, and P. W. M. Blom, Bimolecular recombination in polymer/fullerene bulk heterojunction solar cells, Appl. Phys. Lett. **88**, 052104 (2006).

[52] A. Maurano, R. Hamilton, C. G. Shuttle, A. M. Ballantyne, J. Nelson, B. O'Regan, W. Zhang, I. McCulloch, H. Azimi, M. Morana, C. J. Brabec, and J. R. Durrant, Recombination dynamics as a key determinant of open circuit voltage in organic bulk heterojunction solar cells: A comparison of four different donor polymers, Adv. Mater. **22**, 4987 (2010).

[53] C. G. Shuttle, B. O'Regan, A. M. Ballantyne, J. Nelson, D. D. C. Bradley, and J. R. Durrant, Bimolecular recombination losses in polythiophene: Fullerene solar cells, Phys. Rev. B **78**, 113201 (2008).

[54] C. Deibel and A. Wagenpfahl, Comment on "Interface state recombination in organic solar cells", Phys. Rev. B **82**, 207301 (2010).

[55] J. Benduhn, K. Tvingstedt, F. Piersimoni, S. Ullbrich, Y. Fan, M. Tropiano, K. A. McGarry, O. Zeika, M. K. Riede, C. J. Douglas, S. Barlow, S. R. Marder, D. Neher, D. Spoltore, and K. Vandewal, Intrinsic non-radiative voltage losses in fullerene-based organic solar cells, Nat. Energy **2**, 17053 (2017).

[56] G. Lakhwani, A. Rao, and R. H. Friend, Bimolecular recombination in organic photovoltaics, Annu. Rev. Phys. Chem. **65**, 557 (2014).

[57] G.-J. A. H. Wetzelaer, M. Kuik, and P. W. M. Blom, Identifying the nature of charge recombination in organic solar cells from charge-transfer state electroluminescence, Adv. Energy Mater. **2**, 1232 (2012).

[58] T. Kirchartz, F. Deledalle, P. S. Tuladhar, J. R. Durrant, and J. Nelson, On the differences between dark and light ideality factor in polymer:fullerene solar cells, J. Phys. Chem. Lett. **4**, 2371 (2013).

[59] W. Tress, K. Leo, and M. Riede, Influence of hole-transport layers and donor materials on open-circuit voltage and shape of I-V curves of organic solar cells, Adv. Funct. Mater. **21**, 2140 (2011).

[60] U. Würfel, D. Neher, A. Spies, and S. Albrecht, Impact of charge transport on current-voltage characteristics and power-conversion efficiency of organic solar cells, Nat. Commun. **6**, 6951 (2015).

[61] J. A. Bartelt, D. Lam, T. M. Burke, S. M. Sweetnam, and M. D. McGehee, Charge-carrier mobility requirements for bulk heterojunction solar cells with high fill factor and external quantum efficiency greater 90%, Adv. Energy Mater. **5**, 1500577 (2015).

[62] M. Fox, *Optical Properties of Solids* (Oxford University Press, Oxford, 2002).

[63] P. W. M. Blom, V. D. Mihailetchi, L. J. A. Koster, and D. E. Markov, Device physics of polymer:fullerene bulk heterojunction solar cells, Adv. Mater. **19**, 1551 (2007).

[64] B. Pieters, J. Krc, and M. Zeman, Advanced numerical simulation tool for solar cells-ASA5, in *Proceedings of Photovoltaic Energy Conversion, 2006 IEEE 4th World Conference on Photovoltaic Energy Conference* (IEEE, Piscataway, NJ, 2006), p. 1513.

[65] J. Kniepert, I. Lange, J. Heidbrink, J. Kurpiers, T. J. K. Brenner, L. J. A. Koster, and D. Neher, Effect of solvent additive on generation, recombination, and extraction in PTB7:PCBM solar cells: A conclusive experimental and numerical simulation study, J. Phys. Chem. C **119**, 8310 (2015).

[66] M. M. Mandoc, F. B. Kooistra, J. C. Hummelen, B. de Boer, and P. W. M. Blom, Effect of traps on the performance of bulk heterojunction organic solar cells, Appl. Phys. Lett. **91**, 263505 (2007).

[67] R. A. Street, A. Krakaris, and S. R. Cowan, Recombination through different types of localized states in organic solar cells, Adv. Funct. Mater. **22**, 4608 (2012).

[68] D. Kiermasch, A. Baumann, M. Fischer, V. Dyakonov, and K. Tvingstedt, Revisiting lifetimes from transient electrical characterization of thin film solar cells; a capacitive concern evaluated for silicon, organic and perovskite devices, Energy Environ. Sci. **11**, 629 (2018).

[69] J. A. Röhr, T. Kirchartz, and J. Nelson, On the correct interpretation of the low voltage regime in intrinsic single-carrier devices, J. Phys.: Condens. Matter **29**, 205901 (2017).

[70] A. Melianas and M. Kemerink, Photogenerated charge transport in organic electronic materials: Experiments confirmed by simulations, Adv. Mater. **31**, 1806004 (2019).

[71] O. J. Sandberg, S. Sandén, A. Sundqvist, J.-H. Smått, and R. Österbacka, Determination of Surface Recombination Velocities at Contacts in Organic Semiconductor Devices Using Injected Carrier Reservoirs, Phys. Rev. Lett. **118**, 076601 (2017).

[72] J. A. Röhr, D. Moia, S. A. Haque, T. Kirchartz, and J. Nelson, Exploring the validity and limitations of the Mott–Gurney law for charge-carrier mobility determination of semiconducting thin-films, J. Phys.: Condens. Matter **30**, 105901 (2018).